LETTERS

Nucleation and growth mechanism of ferroelectric domain-wall motion

Young-Han Shin[1]†, Ilya Grinberg[1], I-Wei Chen[2] & Andrew M. Rappe[1]

The motion of domain walls is critical to many applications involving ferroelectric materials, such as fast high-density non-volatile random access memory[1]. In memories of this sort, storing a data bit means increasing the size of one polar region at the expense of another, and hence the movement of a domain wall separating these regions. Experimental measurements of domain growth rates in the well-established ferroelectrics $PbTiO_3$ and $BaTiO_3$ have been performed, but the development of new materials has been hampered by a lack of microscopic understanding of how domain walls move[2–11]. Despite some success in interpreting domain-wall motion in terms of classical nucleation and growth models[12–16], these models were formulated without insight from first-principles-based calculations, and they portray a picture of a large, triangular nucleus that leads to unrealistically large depolarization and nucleation energies[5]. Here we use atomistic molecular dynamics and coarse-grained Monte Carlo simulations to analyse these processes, and demonstrate that the prevailing models are incorrect. Our multi-scale simulations reproduce experimental domain growth rates in $PbTiO_3$ and reveal small, square critical nuclei with a diffuse interface. A simple analytic model is also proposed, relating bulk polarization and gradient energies to wall nucleation and growth, and thus rationalizing all experimental rate measurements in $PbTiO_3$ and $BaTiO_3$.

Symmetry breaking by an external electric field on a 180° ferroelectric domain wall leads to domain-wall motion. The domain-wall speed has been found to be proportional to $\exp(-E_a/E)$ (Merz's law), where E_a is the 'activation field' and E is the applied electric field[2]. A classic theory supporting Merz's law was developed by Miller and Weinreich[15]. They suggested that the critical nucleus is an atomically thin triangular plate with a large aspect ratio, which then expands laterally on the same atomic plane[15]. However, the experimental and theoretical observations have shown that the Miller–Weinreich theory overestimates the activation field by an order of magnitude[5,17]. Thus, the details of the intrinsic properties and the mechanism of the domain dynamics are still unclear. This is due to experimental limitations in detecting rapid polarization changes in small regions and the computational difficulty of accurately simulating a sufficiently large supercell. Therefore, there is currently a gap between experimental measurements that probe domain-wall propagation (the result of nucleation and growth), and classical theories that focus on nucleation. This has motivated us to study domain-wall motion with molecular dynamics simulations[18,19] and for longer times and a larger length scale we model it with coarse-grained Monte Carlo simulations. This approach enables us to obtain the domain-wall speed in $PbTiO_3$ without the effect of defects and grain boundaries, giving the upper bound of the wall speed of real thin films.

Molecular dynamics simulations allow us precisely to isolate and study the nucleation aspect of the domain-wall motion. When an external field is applied (Fig. 1a and 1b), critical nuclei randomly form on the domain wall. A critical nucleus corresponds to the transition state between the reactant (the domain-wall layer polarized negatively, opposite to the applied field direction) and the product (the domain-wall layer polarized positively, along the applied field direction). This state of the system is found by analysing the trajectories of the positively polarized nuclei that appear on the domain wall; for a critical nucleus, the probabilities of nucleus growth and disappearance are the same. Nucleation was found to behave as a Poisson process, in that the probability that no critical nucleus has formed exponentially decreases with time t (Fig. 1c). This permits the extraction of a nucleation rate J from the molecular dynamics data.

For small supercells, interaction between periodic images may give rise to artefacts. To eliminate this problem, we carried out a series of domain-wall motion studies on supercells, increasing the wall area from $(3\times3)ac$ to $(6\times6)ac$, where a and c are the lattice constants of tetragonal $PbTiO_3$. The third dimension was kept constant at $18a$. For all temperatures, the nucleation rate converges when reaching $(6\times6)ac$ wall area (Fig. 1d). The rapid convergence of the nucleation rate J with cell size allows us to determine the simulation-area-independent, steady-state nucleation rate $J(T,E)$ for various temperatures T and applied electric fields E as presented in Table 1. Analysis of these results reveals that nucleation follows Merz's law with an activation field $E_{a,n}$ of 1.2–6.7 MV cm^{-1} over the 200–300 K temperature range.

Molecular dynamics simulations also show that the growth of critical nuclei is two-dimensional, with activation barriers much smaller than for nucleation. We identify six growth rates $G_{m,n}$, distinguished by the polarization of the four nearest neighbours around each five-atom unit cell on the domain wall. In this notation, m (or n) denotes the number of sideways (or forward) neighbours whose polarity is the same as the field direction (Fig. 2a). These growth rates are extracted from simulations with large domain-wall areas by digitizing the local polarizations on the domain wall, treating all cells with $P_z \geq 0$ as positively polarized neighbours and $P_z < 0$ as negatively polarized neighbours. We find that growth is also an activated process following Merz's law, with an activation field $E_{a,g}$ around 0.6–1.1 MV cm^{-1} over the 200–300 K temperature range for the slowest growth rate $G_{1,0}$ (Table 1).

Combining the molecular dynamics results for nucleation and growth processes, we used coarse-grained Monte Carlo simulations to model domain-wall propagation. We define the overall domain-wall speed v as the rate of increase in up-polarized domain volume divided by the wall area of the initial up-polarized domain. The obtained values for the total domain-wall speed v are shown in Fig. 2b. The speed also follows Merz's law with an activation field $E_{a,t}$ of 0.8–3.2 MV cm^{-1} over the 200–300 K temperature range. At lower field strengths, we find good agreement between our domain-wall velocities and room-temperature experimental data[5,8,11]. Additionally, the activation fields

[1]The Makineni Theoretical Laboratories, Department of Chemistry, University of Pennsylvania, Philadelphia, Pennsylvania 19104–6323, USA. [2]Department of Materials Science and Engineering, University of Pennsylvania, Philadelphia, Pennsylvania 19104–6272, USA. †Present address: Department of Materials Science and Engineering, Pohang University of Science and Technology, Pohang 790–784, Korea.

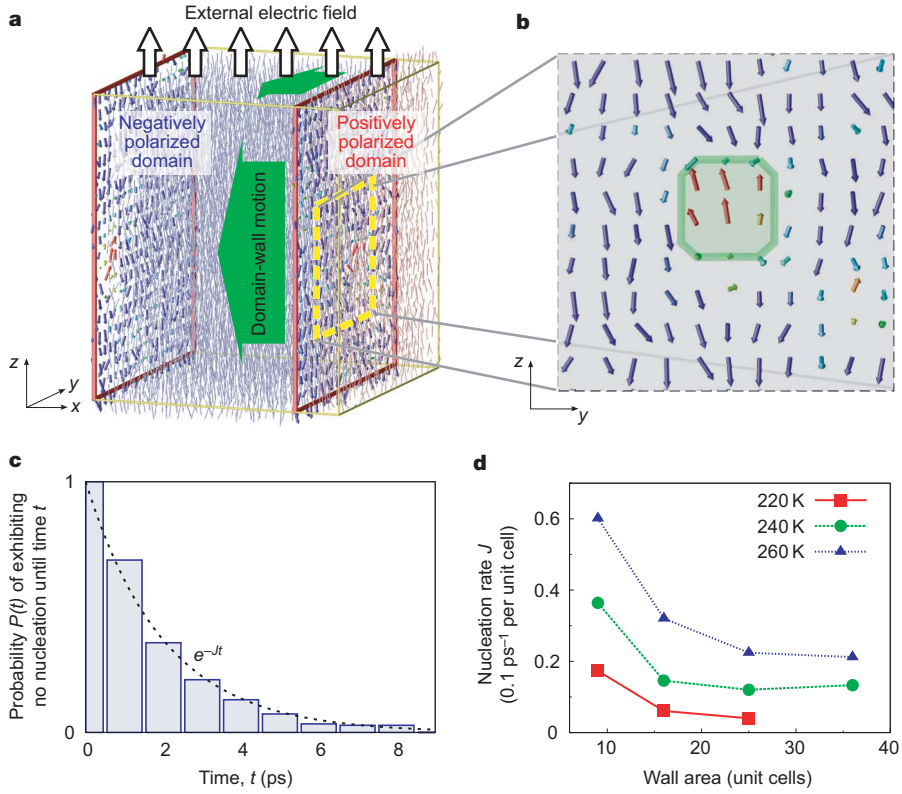

Figure 1 | Molecular dynamics simulations of nucleation on 180° domain walls. **a**, A snapshot of the polarization from a molecular dynamics simulation of $PbTiO_3$ at 220 K and 0.5 MV cm^{-1}. The local polarization vectors are shown by the red and blue arrows. The two domain walls are outlined with red lines. **b**, A critical nucleus on the domain wall on the *y*–*z* plane. The green solid line shows the boundary of the critical nucleus. **c**, The fraction of the simulations exhibiting no nucleation by time *t*. The exponent of the fit function corresponds to the nucleation rate *J*. **d**, Size dependence of the nucleation rates on the (100) 180° domain wall.

$E_{a,t}$ are in excellent accord with the experimental results of Tybell *et al.*[5] for $Pb(Zr_{0.2}Ti_{0.8})O_3$ films (~1.0 MV cm^{-1} at room temperature). The activation field of the overall wall velocity also agrees with the Avrami theory of transformation kinetics, which predicts the overall activation field to be roughly the weighted average of the nucleation and growth activation fields. That is, $E_{a,t} = 1/(d+1)E_{a,n} + d/(d+1)E_{a,g}$, where d is dimensionality, which is approximately 2 in our case[13].

For the nucleation process, our results are in gross disagreement with the Miller–Weinreich theory predictions (using $P_s = 0.76$ C m^{-2}, dielectric constant $\varepsilon = 60$ and a (100) domain-wall energy $\sigma_{100} = 0.11$ J m^{-2}): critical width $l_y = 43$ Å, critical height $l_z = 53$ Å and $E_{a,n} = 40$ MV cm^{-1} at $E = 0.5$ MV cm^{-1} and $T = 240$ K. Such a high activation field would lead to a domain-wall velocity many orders of magnitude smaller than that observed in experiments or our simulations. This reconfirms the well-known disagreement between the Miller–Weinreich predictions of the activation energy and field and the experimental observations. Detailed examination of the critical nuclei using large 20 × 20 supercells reveals further significant discrepancies between our molecular dynamics results and the traditional Miller–Weinreich model of nucleation. A snapshot of the polarization reversal process (Fig. 1b) portrays a 12 Å × 12 Å critical nucleus that is nearly square, not triangular in shape. Figure 1b also shows considerable diffuseness, in contrast to the sharp polarization reversal in the nucleus assumed by the Miller–Weinreich theory.

We therefore develop an analytic model to relate computed and experimental domain-wall velocities to material properties that are easily obtained from bulk experimental data or from static density functional theory (DFT) calculations. We base our nucleation model on the Landau–Ginzburg–Devonshire approach. Here, the structure at the domain wall is due to interplay between two energy terms. The first term reflects the local energy cost for the polarization to deviate from the spontaneous polarization P_s

$$U_{loc}(P_z) = A_{loc}\left[1 - \left(\frac{P_z}{P_s}\right)^2\right]^2 \quad (1)$$

where the constant A_{loc} is 3.55×10^8 J m^{-3} at 0 K for our atomistic model and decreases with temperature as $P_s^4(T)$. This term is zero for a sharp polarization reversal from P_s to $-P_s$, but rises with diffuseness. The second term represents the preference of electric dipoles to align, associating higher gradient energy with larger polarization gradients

$$U_m(P_z) = g_m\left(\frac{\partial P_z}{\partial m}\right)^2 \quad (2)$$

Table 1 | Nucleation and growth rates and activation fields

T (K)	*E* = 0.45 MV cm^{-1}		*E* = 0.50 MV cm^{-1}		*E* = 0.55 MV cm^{-1}		*E* = 0.60 MV cm^{-1}		*E* = 0.65 MV cm^{-1}		Activation field		
	J	$G_{1,0}$	*J*	$G_{1,0}$	*J*	$G_{1,0}$	*J*	$G_{1,0}$	*J*	$G_{1,0}$	$E_{a,n}$	$E_{a,g}$	$E_{a,t}$
200					1.9	12.4	5.8	13.7			6.7	1.1	3.2
220			3.2	13.2	8.5	14.7	18.2	16.4	29.9	20.1	4.9	0.9	2.1
240	5.0	12.3	11.0	15.8	22.5	17.6	33.6	20.9	47.6	23.3	3.3	0.9	1.5
260	14.7	16.9	25.2	18.4	38.8	20.6	50.0	21.4	62.5	24.0	1.9	0.5	1.0
280	27.6	17.8	40.4	19.0	51.3	22.9	63.8	23.9			1.5	0.6	0.9
300	40.2	21.0	55.2	23.7	65.9	25.7	77.7	29.0			1.2	0.6	0.8

The nucleation rate *J* is measured in 10^{-3} ps^{-1} per unit cell and the growth rate $G_{1,0}$ is measured in ps^{-1} per unit cell.

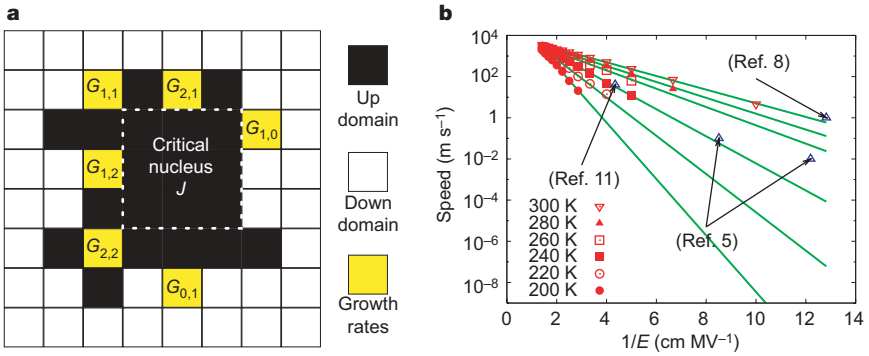

Figure 2 | Coarse-grained Monte Carlo simulations of polarization switching. a, Definition of growth rates. $G_{m,n}$ means the rate of the event of changing the polarization of a unit cell, which has m sideways neighbours and n forward neighbours polarized along the field direction. Here the direction of the field is 'up'. Growth rates $G_{m,n}$ can be deduced from counting the required time for flipping yellow unit cells. **b**, The overall domain-wall speeds as a function of T and E. They are comparable to recent experiments and conform to Merz's law: speed $v \approx \exp(-E_{a,t}/E)$.

where g_m is the gradient coefficient along the m direction. According to our molecular dynamics simulations, the coefficient along the polar axis g_z is 1.07×10^{11} m^3 F^{-1}, and the coefficients normal to the polar axis g_x and g_y are 0.63×10^{-11} m^3 F^{-1} (see Methods). The energy difference ΔU in a two-dimensional nucleus on the domain wall relative to the domain wall without any nucleus can be expressed as a function of its size l_y and l_z, and the z-component of the local polarization $P_z(x, y, z)$:

$$\Delta U = \Delta U_v + \Delta U_i \quad (3)$$

$$\Delta U_v = -E \int_{-\infty}^{\infty} dx \int_{-\infty}^{\infty} dy \int_{-\infty}^{\infty} dz \left(P_z(x, y, z) - P_z^{180}(x, y, z)\right) \quad (4)$$

$$\Delta U_i = \int_{-\infty}^{\infty} dx \int_{-\infty}^{\infty} dy \int_{-\infty}^{\infty} dz \left\{ \left[U_x(P_z) + U_y(P_z) + U_z(P_z) + U_{loc}(P_z)\right] - \left[U_x(P_z^{180}) + U_{loc}(P_z^{180})\right] \right\} \quad (5)$$

Here P_z^{180} is the polarization of the clean 180° domain wall without any nucleus on it, and the reversal of $P_z(x, y, z)$ around the nucleus is spread across a diffuse interface with the lateral diffuseness parameters δ_y and δ_z and the transverse diffuseness parameter δ_x. The critical nucleus is then obtained by numerically locating the saddle point of ΔU. Using the polarization and A_{loc} values appropriate for our model potential, we find $l_y = 12$ Å, $l_z = 12$ Å, $\delta_y = 3.9$ Å, $\delta_z = 4.6$ Å at $T = 240$ K and $E = 0.5$ MV cm^{-1} (Supplementary Fig. 5a), in agreement with the microscopic nucleus structure shown in Fig. 1b. We also obtain the activation fields $E_{a,n}$ in excellent agreement with simulation results for the whole 200–300 K range of simulations (Fig. 3c). We further obtain $\delta_x = 3.5$ Å, indicating the nucleus is still very much limited to one atomic plane despite lateral diffuseness.

The much smaller l_y, l_z and $E_{a,n}$ are due to three new features, which are absent in the Miller–Weinreich model. First, the amount of the interface area for any nucleus is significantly less than the Miller–Weinreich model estimate due to lateral diffuseness. In the Miller–Weinreich model (Fig. 3a), nucleation creates additional domain-wall area of Sa (lattice constants $a = 3.9$ Å and $c = 4.15$ Å, $c/a \approx 1$, and S is the nucleus perimeter). The domain wall passes through all atoms with $P_z = 0$, and between neighbouring up- and down-polarized atoms. In the new model, Pb off-centring (A–D in Fig. 3b) allows a slanted (101) domain wall of area $Sa\sqrt{2}$ to replace the flat wall area (Sa), resulting in net wall creation of $Sa(\sqrt{2} - 1) \approx 0.4Sa$. Second, in contrast to full up- and down-polarizations at two adjacent sites in the Miller–Weinreich model, our model places smaller polarizations at these sites, reducing the polarization gradient, and hence the gradient energy, by 50%. The energy per unit area of the interface is lower than in the Miller–Weinreich model because polarization changes with the finite diffuseness parameters δ_y and δ_z, and P_z is smaller than P_s. Taken together, these effects show that for the same nucleus perimeter, the interface energy cost is a factor of three to four lower than that estimated by the Miller–Weinreich theory, directly leading to an order-of-magnitude reduction in critical nucleus area and energy.

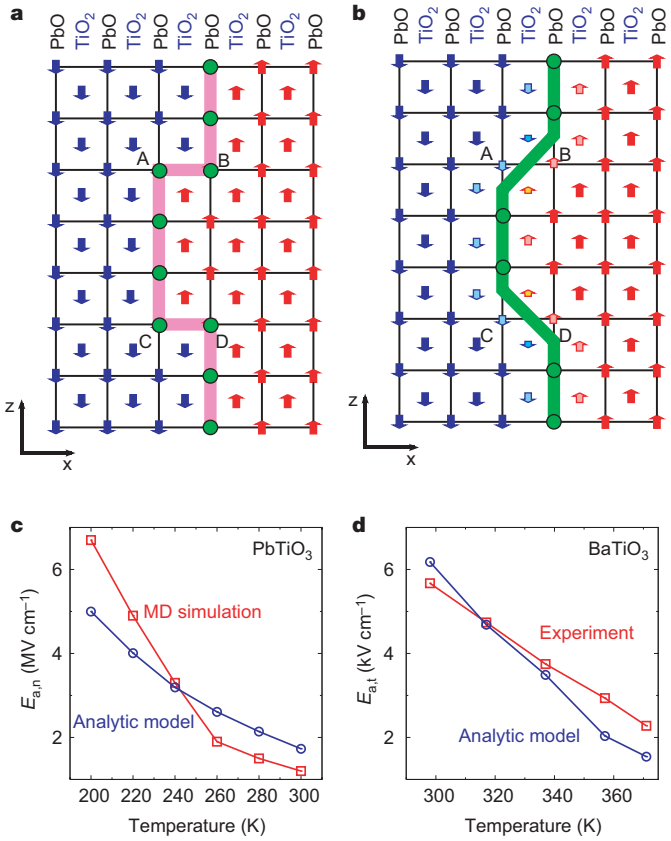

Figure 3 | Landau-Ginzburg-Devonshire model of nucleation on 180° domain walls. a, **b**, Schematic diagrams of the Miller–Weinreich model (**a**) and the diffuse-boundary model (**b**) on the x–z plane, with $P_z = 0$ marked by circles and Pb off-centring at A–D. In the Miller–Weinreich picture, all the Pb atoms at the nucleus boundary (circled in **a**) have no off-centre displacement, as shown by the lack of arrows along the z direction. In the Landau–Ginzburg–Devonshire model, the edge of the nucleus boundary bypasses the Pb atoms (A–D in **b**) that are polarized in the asymmetric environment. **c**, Comparison of the activation fields obtained from simulations of $PbTiO_3$ (squares) with the results of the Landau–Ginzburg–Devonshire model (circles). **d**, Comparison of the activation fields obtained experimentally (ref. 22) for $BaTiO_3$ (squares) with the results of the Landau–Ginzburg–Devonshire model (circles).

Third, since the critical nucleus is small, the depolarization energy is not important during the nucleation process. This enables the formation of square nuclei instead of triangular ones.

Because our model can predict $E_{a,n}$ without any molecular dynamics simulations, we have extended it to $BaTiO_3$ using only experimental P_s and energies obtained by DFT calculations. In our theory, four parameters are necessary for modelling nucleation at a given temperature T: g_x, g_z, A_{loc} and $P_s(T)$. From five-atom bulk $BaTiO_3$ DFT calculations with the local density approximation in the literature, we obtain $A_{loc} = 9.5$ meV per unit cell[20]. The 180° (100) domain-wall energy is $\sigma_{100} = 6$–$7.5\ mJ\ m^{-2}$ according to the DFT calculations in refs 17 and 21. The P_s of tetragonal $BaTiO_3$ is $0.31\ C\ m^{-2}$ at 0 K and its temperature dependence is given by ref. 22. From these data, we can obtain $g_x = 0.22 \times 10^{-11}\ m^3\ F^{-1}$ (see Methods). Using this g_x value for $BaTiO_3$ and the ratio between g_x and g_z determined for $PbTiO_3$, we estimate $g_z = 0.38 \times 10^{-11}\ m^3\ F^{-1}$. Our Landau–Ginzburg–Devonshire model then predicts $E_{a,n}$ values of 4.6–18.5 kV cm^{-1} for the 298–371 K temperature range. According to the Avrami equation, $E_{a,t}$ should be larger than $E_{a,n}/3$. This allows us to obtain a lower bound for $E_{a,t}$ values that compares well with the experimental data of ref. 22, as shown in Fig. 3d, indicating very fast growth in $BaTiO_3$ in these experiments. In contrast, using the DFT-obtained domain-wall energy, the Miller–Weinreich theory would predict $E_{a,n} = 240\ kV\ cm^{-1}$ for $T = 300$ K, which is clearly out of the question.

In conclusion, our multi-scale modelling finds domain-wall velocities in agreement with the most direct experimental evidence for related materials. It also allows the construction of a general and accurate model for a critical nucleus. Together, they provide microscopic insight into how the changes in the nucleus shape and polarization profile can dramatically lower activation barriers.

METHODS SUMMARY

We studied many $PbTiO_3$ structures with first-principles DFT, and these provided a database of energies and forces for calibrating an inter-atomic potential which was based on Brown's rules of valence[23]. The molecular dynamics simulations exhibited fundamental domain-wall processes, including critical nucleus formation and growth. Initially, three layers were polarized up and 15 layers were polarized down, and each layer had $N_y \times N_z$ unit cells. After equilibrating the system, we applied the electric field in the range of 0.45 to 0.65 MV cm^{-1} under the Nosé–Hoover thermostat with a 1 fs time step. Nucleation is a stochastic process, so nucleation rates were obtained from the statistics of molecular dynamics simulations. Two hundred randomly dispersed initial coordinates were used to determine each nucleation rate. To model larger-scale, longer-time domain-wall motion processes, we simulated phase transformation of ferroelectric domains with the nucleation-and-growth model[13,19,24–26]. The local polarization of each primitive five-atom $PbTiO_3$ unit cell was chosen as a unit in this coarse-grained Monte Carlo simulation, while the nucleation and growth rates were obtained from the analysis of the molecular dynamics simulations.

The overall domain-wall speed v can be obtained from the Monte Carlo study using the following relation $v = \frac{1}{NA}\frac{\partial V_{up}}{\partial t} = \frac{d_1}{N}\frac{\partial}{\partial t}\sum_l q_l(t)$, where $V_{up} = Ad_1\sum_l q_l(t)$ is the up-polarized domain volume, A is the wall area, $d_1 \approx a$ is the distance between adjacent layers, q_l is the normalized polarization fraction of the lth layer, and N is the number of domain walls ($N = 2$ owing to the periodic boundary conditions in our coarse-grained Monte Carlo simulations). Such a multiscale strategy enabled us to increase the system size to the micrometre scale and accurately evaluate the overall domain-wall-motion speed.

Full Methods and any associated references are available in the online version of the paper at www.nature.com/nature.

Received 11 April; accepted 6 August 2007.
Published online 7 October 2007.

1. Scott, J. F. & Paz de Araujo, C. A. Ferroelectric memories. *Science* **246,** 1400–1405 (1989).
2. Merz, W. J. Domain formation and domain wall motions in ferroelectric $BaTiO_3$ single crystals. *Phys. Rev.* **95,** 690–698 (1954).
3. Stadler, H. L. & Zachmanidis, P. J. Nucleation and growth of ferroelectric domains in $BaTiO_3$ at fields from 2 to 450 kV/cm. *J. Appl. Phys.* **34,** 3255–3260 (1963).
4. Ganpule, C. S. *et al.* Role of 90° domains in lead zirconate titanate thin films. *Appl. Phys. Lett.* **77,** 292–294 (2000).
5. Tybell, T., Paruch, P., Giamarchi, T. & Triscone, J.-M. Domain wall creep in epitaxial ferroelectric $Pb(Zr_{0.2}Ti_{0.8})O_3$ thin films. *Phys. Rev. Lett.* **89,** 097601 (2002).
6. Ahn, C. H., Rabe, K. M. & Triscone, J.-M. Ferroelectricity at the nanoscale: local polarization in oxide thin films and heterostructures. *Science* **303,** 488–491 (2004).
7. Li, J. *et al.* Ultrafast polarization switching in thin-film ferroelectrics. *Appl. Phys. Lett.* **84,** 1174–1176 (2004).
8. Gruverman, A. *et al.* Direct studies of domain switching dynamics in thin film ferroelectric capacitors. *Appl. Phys. Lett.* **87,** 082902 (2005).
9. So, Y. W., Kim, D. J., Noh, T. W., Yoon, J.-G. & Song, T. K. Polarization switching kinetics of epitaxial $Pb(Zr_{0.4}Ti_{0.6})O_3$ thin films. *Appl. Phys. Lett.* **86,** 092905 (2005).
10. Stolichnov, I., Malin, L., Colla, E., Tagantsev, A. K. & Setter, N. Microscopic aspects of the region-by-region polarization reversal kinetics of polycrystalline ferroelectric $Pb(Zr,Ti)O_3$ films. *Appl. Phys. Lett.* **86,** 012902 (2005).
11. Grigoriev, A. *et al.* Nanosecond domain wall dynamics in ferroelectric $Pb(Zr,Ti)O_3$ thin films. *Phys. Rev. Lett.* **96,** 187601 (2006).
12. Landauer, R. Electrostatic considerations in $BaTiO_3$ domain formation during polarization reversal. *J. Appl. Phys.* **28,** 227–234 (1957).
13. Shur, V., Rumyantsev, E. & Makarov, S. Kinetics of phase transformations in real finite systems: application to switching in ferroelectrics. *J. Appl. Phys.* **84,** 445–451 (1998).
14. Hayashi, M. Kinetics of domain wall motion in ferroelectric switching. I. General formation. *J. Phys. Soc. Jpn* **33,** 616–628 (1972).
15. Miller, R. C. & Weinreich, G. Mechanism for the sidewise motion of 180° domain walls in barium titanate. *Phys. Rev.* **117,** 1460–1466 (1960).
16. Orihara, H., Hashimoto, S. & Ishibashi, Y. A theory of *D-E* hysterisis loop based on the Avrami model. *J. Phys. Soc. Jpn* **63,** 1031–1035 (1994).
17. Padilla, J., Zhong, W. & Vanderbilt, D. First-principles investigation of 180° domain walls in $BaTiO_3$. *Phys. Rev. B* **53,** R5969–R5973 (1996).
18. Grinberg, I., Cooper, V. R. & Rappe, A. M. Relationship between local structure and phase transitions of a disordered solid solution. *Nature* **419,** 909–911 (2002).
19. Shin, Y.-H., Cooper, V. R., Grinberg, I. & Rappe, A. M. Development of a bond-valence molecular-dynamics model for complex oxides. *Phys. Rev. B* **71,** 054104 (2005).
20. Cohen, R. E. Origin of ferroelectricity in perovskite oxides. *Nature* **358,** 136–138 (1992).
21. Meyer, B. & Vanderbilt, D. *Ab initio* study of ferroelectric domain walls in $PbTiO_3$. *Phys. Rev. B* **65,** 104111 (2002).
22. Savage, A. & Miller, R. C. Temperature dependence of the velocity of sidewise 180° domain-wall motion in $BaTiO_3$. *J. Appl. Phys.* **31,** 1546–1549 (1960).
23. Brown, I. D. & Wu, K. K. Empirical parameters for calculating cation-oxygen bond valences. *Acta Crystallogr.* **B32,** 1957–1959 (1976).
24. Avrami, M. Kinetics of phase change. I. General theory. *J. Phys. Chem.* **7,** 1103–1112 (1939).
25. Kashchiev, D. *Nucleation: Basic Theory with Applications* Ch. 26 (Butterworth-Heinemann, Woburn, Massachusetts, 2000).
26. Lines, M. E. & Glass, A. M. *Principles and Applications of Ferroelectrics and Related Materials* Ch. 4 (Clarendon Press, Oxford, 1977).

Supplementary Information is linked to the online version of the paper at www.nature.com/nature.

Acknowledgements This material is based upon work supported by the US Office of Naval Research, the National Science Foundation and the Army Engineer Research and Development Center. Computational support was provided by the US Department of Defense. Y.-H.S. was supported by the Brain Korea 21 project in 2006.

Author Information Reprints and permissions information is available at www.nature.com/reprints. The authors declare no competing financial interests. Correspondence and requests for materials should be addressed to A.M.R. (rappe@sas.upenn.edu).

METHODS

Here we explain the details of the analytical model of the critical nucleus on the ferroelectric domain wall, as well as our procedure for extracting the model coefficients from molecular dynamics simulations. The model discussed here closely follows the treatment in ref. 26.

Total free energy. The total free energy difference of a stripe domain is:

$$G - G_0 = W_g + W_E + W_e + W_l \tag{6}$$

where G_0 is the single domain free energy, W_g is the gradient energy due to the dipole-dipole interaction, W_E is the depolarizing energy, W_e is the elastic energy, and W_l is the local energy contribution from the Landau–Ginzburg–Devonshire phenomenological theory. Two minima of $E(P) = 1/2AP^2 + 1/4BP^4$ where $A = A_0(T - T_c)$, $A_0 > 0$, and $B > 0$ are located at $P_s = \pm\sqrt{(-A/B)}$, and the local energy W_l can be expressed as:

$$W_l = \iiint U_{loc}(P(x,y,z))\,dx dy dz \tag{7}$$

where $P(x, y, z)$ is the magnitude of a general polarization vector $\boldsymbol{P}(x, y, z)$, and the local energy per unit cell $U_{loc}(P)$ is:

$$\begin{aligned} U_{loc}(P(x,\,y,\,z;\;T)) &= E(P(x,\,y,\,z;\;T)) - E(P_s(T)) \\ &= \left(\frac{1}{2}AP^2 + \frac{1}{4}BP^4\right) - \left(\frac{1}{2}AP_s^2 + \frac{1}{4}BP_s^4\right) \\ &= \left(\frac{1}{2}(-BP_s^2)P^2 + \frac{1}{4}BP^4\right) - \left(\frac{1}{2}(-BP_s^2)P_s^2 + \frac{1}{4}BP_s^4\right) \\ &= A_{loc}(T)\left(1 - \left(\frac{P(x,\,y,\,z;\;T)}{P_s(T)}\right)^2\right)^2 \end{aligned} \tag{8}$$

where $A_{loc}(T) = -E(P_s(T)) = 1/4BP_s^4(T)$ is the energy difference per unit cell between the relaxed tetragonal ferroelectric phase and the high-symmetry tetragonal paraelectric phase, and P_s is the spontaneous polarization. For the 180° (100) domain wall, only the gradient energy W_g and the local energy W_l remain if we neglect the effect due to the free charge on the crystal surfaces.

Extracting model parameter from the (100) domain-wall energy. The 180° domain-wall energy σ_{100} is given by

$$\sigma_{100} = \frac{E_{100}^{2m\times1\times1} - E_{mono}^{2m\times1\times1}}{2A_{100}} = \frac{W_g + W_l}{2A_{100}} \tag{9}$$

where A_{100} is the area of the domain wall whose normal vector is [1 0 0] ($A_{100} = ac$ for the $2m \times 1 \times 1$ supercell, and a and c are the lattice constants ($a < c$)). $E_{100}^{2m\times1\times1}$ is the total energy of up–down domains, and $E_{mono}^{2m\times1\times1}$ is the total energy of a single domain. In the energy calculation, one supercell is composed of $2m \times 1 \times 1$ unit cells. Because we used periodic boundary conditions in this calculation, there are two domain walls in a supercell, which is the reason for the 2 in the denominator of equation (9). The spontaneous polarization P_s of $PbTiO_3$ is 0.89 C m^{-2} at 0 K, and the polarization next to the domain wall P_b is smaller than P_s; the diffuseness parameter (or domain-wall width) δ_x is approximately one unit cell. The polarization $P_z(x)$ across the domain wall looks like $-P_s, \ldots, -P_s, -P_b, 0, P_b, P_s, \ldots, P_s$, where $P_s = 0.89$ C m^{-2} and $P_b = 0.73$ C m^{-2} (Supplementary Table 2).

From the Landau–Ginzburg–Devonshire model with gradient terms, the polarization around the clean 180° (100) domain-wall boundary P_0 can be expressed with the hyperbolic function:

$$P_o(x,\,y,\,z) = P_s \tanh\left(\frac{x}{\delta_x/2}\right) = p(x) \tag{10}$$

which is shown in Supplementary Fig. 1. The parameter δ_x is the domain-wall width found by fitting the polarization data across the domain wall to equation (10).

Following equations (8) and (10), σ_{100} from the $2m \times 1 \times 1$ super cell can be expressed as:

$$\sigma_{100} = \left(W_l^{100} + W_{gx}^{100}\right)/(2A_{100}) \tag{11}$$

$$\begin{aligned} W_l^{100} &= \int_{-ma}^{ma} dx \int_{-a/2}^{a/2} dy \int_{-c/2}^{c/2} dz\; U_{loc}(P_{0,z}(x,\,y,\,z)) = ac \int_{-ma}^{ma} U_{loc}(p)dx \\ &= ac \int_{-P_s}^{P_s} \frac{dp}{\frac{2}{\delta_x}\frac{P_s^2 - p^2}{P_s}} A_{loc}\left(1 - \left(\frac{p}{P_s}\right)^2\right)^2 = \frac{acA_{loc}\delta_x}{2P_s^3}\int_{-P_s}^{P_s}\left(P_s^2 - p^2\right)dp \\ &= \frac{2}{3}acA_{loc}\delta_x \end{aligned} \tag{12}$$

$$\begin{aligned} W_{gx}^{100} &= g_x \int_{-c/2}^{c/2} dz \int_{-a/2}^{a/2} dy \int_{-ma}^{ma} dx \left(\frac{dp}{dx}\right)^2 \\ &= g_x \int_{-P_s}^{P_s} \left(\frac{dp}{dx}\right) dp = \frac{2g_x ac}{\delta_x P_s}\int_{-P_s}^{P_s}(P_s^2 - p^2)dp \\ &= \frac{8ac}{3\delta_x}P_s^2 g_x \end{aligned} \tag{13}$$

where the factor 2 in the denominator of equation (11) is due to two domain walls per supercell. By $\partial\sigma_{100}/\partial\delta_x\big|_{\delta_x = \delta_x^*} = 0$, the diffuseness parameter δ_x^* and the gradient coefficient g_x are

$$\delta_x^* = 2P_s\sqrt{\frac{g_x}{A_{loc}}} \tag{14}$$

$$\sigma_{100} = \frac{8P_s}{3}\sqrt{g_x A_{loc}} \tag{15}$$

$$g_x = \left(\frac{3\sigma_{100}}{8P_s}\right)^2 \frac{1}{A_{loc}} \tag{16}$$

σ_{100} and P_s are obtained from molecular dynamics simulations, and they are 0.125 J m^{-2} and 0.89 C m^{-2}, respectively. We use $A_{loc} = 3.55 \times 10^8$ J m^{-3} or 0.14 eV per unit cell for $PbTiO_3$ at 0 K. From these values and from equation (16), g_x equals 0.63×10^{-11} m^3 F^{-1}. By integrating equation (13) numerically with the polarization from molecular dynamics simulations, we obtain $g_x = 0.58 \times 10^{-11}$ m^3 F^{-1}. We attribute the small discrepancy between the two estimates to the difference between the continuous and discrete polarization.

Extracting model parameter from the (n01) domain-wall energy σ_{n01}. The 180° (n01) domain-wall energy σ_{n01} of the higher-index interface is:

$$\sigma_{n01} = \frac{E_{n01}^{2m\times1\times n} - E_{mono}^{2m\times1\times n}}{2A_{n01}} \tag{17}$$

where A_{n01} is the area of the $2m \times 1 \times n$ stepped domain wall whose normal vector is [n 0 1] and $A_{n01} = a\sqrt{a^2 + (nc)^2}$. The 180° ($n$01) domain wall is shown in Supplementary Fig. 2a. With an assumption that $P_x(x, y, z) = P_y(x, y, z) = 0$, σ_{n01} can be expressed as:

$$\sigma_{n01} = (W_l + W_{gx} + W_{gz})/(2A_{n01}) \tag{18}$$

$$W_l = \int_{-ma}^{ma} dx \int_{-a/2}^{a/2} dy \int_{-nc}^{nc} dz\; U_{loc}(P_z(x,\,y,\,z)) \tag{19}$$

$$W_{gx} = g_x \int_{-ma}^{ma} dx \int_{-a/2}^{a/2} dy \int_{-nc}^{nc} dz \left(\frac{\partial P_z(x,y,z)}{\partial x}\right)^2, \tag{20}$$

$$W_{gz} = g_z \int_{-ma}^{ma} dx \int_{-a/2}^{a/2} dy \int_{-nc}^{nc} dz \left(\frac{\partial P_z(x,\,y,\,z)}{\partial z}\right)^2 \tag{21}$$

where $\sigma_{n01} = 0.117$ J m^{-2}. From the numerical calculations, we can determine the gradient coefficient g_z as a function of n. We find that g_z converges to 1.07×10^{-11} m^3 F^{-1} as n and m increase (Supplementary Fig. 2b).

Model of the nucleus on the domain wall. To describe the diffuse polarization profile around the nucleus on the domain wall, equation (10) can be generalized as:

$$\begin{aligned} P_z(x,\,y,\,z) &= P_s\left(f^-(x,\,l_x,\,\delta_x)\left(2\frac{f^-(y,\,l_y,\,\delta_y)f^-(z,\,l_z,\,\delta_z)}{f^-(0,\,l_y,\,\delta_y)f^-(0,\,l_z,\,\delta_z)} - 1\right) + f^+(x,\,l_x,\,\delta_x)\right) \\ &\approx 2P_s f^-(x,\,l_x,\,\delta_x)f^-(y,\,l_y,\,\delta_y)f^-(z,\,l_z,\,\delta_z) + P_z^{180}(x - l_x/2,\,y,\,z) \end{aligned} \tag{22}$$

where $f^{\pm}(\alpha, \beta, \gamma) = \frac{1}{2}\tanh\left(\frac{\alpha+\beta/2}{\gamma/2}\right) \pm \frac{1}{2}\tanh\left(\frac{\alpha-\beta/2}{\gamma/2}\right)$, l_k corresponds to the length of the nucleus to the k direction, and δ_k corresponds to the diffuseness parameter along the k direction. The polarization profile generated by equation (22) is shown in Supplementary Fig. 4. When the external field E is applied to the 180° domain wall, the free energy change ΔU from the formation of a nucleus is

$$\Delta U = \Delta U_v + \Delta U_i \tag{23}$$

$$\Delta U_{\mathrm{v}} = -E \int_{-\infty}^{\infty}\int_{-\infty}^{\infty}\int_{-\infty}^{\infty} \mathrm{d}x\mathrm{d}y\mathrm{d}z \left(P_z(x, y, z) - P_z^{180}(x, y, z)\right) \tag{24}$$

$$\Delta U_{\mathrm{i}} = \int_{-\infty}^{\infty}\int_{-\infty}^{\infty}\int_{-\infty}^{\infty} \mathrm{d}x\mathrm{d}y\mathrm{d}z \left\{ \left[g_x\left(\frac{\partial P_z}{\partial x}\right)^2 + g_y\left(\frac{\partial P_z}{\partial y}\right)^2 + g_z\left(\frac{\partial P_z}{\partial z}\right)^2 + U_{\mathrm{loc}}(P_z)\right] - \left[g_x\left(\frac{\partial P_z^{180}}{\partial x}\right)^2 + U_{\mathrm{loc}}\left(P_z^{180}\right)\right]\right\} \tag{25}$$

where $U_{\mathrm{loc}}(p) = A_{\mathrm{loc}}\left(1-(p/p_{\mathrm{s}})^2\right)^2$ and the subscripts v and i mean volume and interface, respectively. We ignore the charge on the nucleus, which is justified, a posteriori, because the depolarization energy in the Miller–Weinreich model is strongly dependent on size, and is negligible when the nucleus is very small. Because we can also find the bulk polarization P_{s} from our model potential, the temperature dependence of $A_{\mathrm{loc}}(T)$ can be deduced from A_{loc} at 0 K and P_{s} at finite temperature.

Using the gradient parameters from the (100) and (n01) domain walls ($g_x = g_y = 0.63 \times 10^{-11}\,\mathrm{m^3\,F^{-1}}$ and $g_z = 1.07 \times 10^{-11}\,\mathrm{m^3\,F^{-1}}$), we can obtain the following results. The aspect ratio of the critical nucleus is close to 1. The critical diffuseness parameter along the polar axis δ_z^* is 4.6 Å, while the diffuseness parameter along the y axis δ_y^* is 3.5 Å. The size of the critical nucleus from this model is 3×3 unit cells and the activation barrier is 0.14 eV at 240 K and 500 kV cm^{-1}. This result is consistent with the molecular dynamics simulations, where we found that the activation energy is about 0.1 eV, and the critical nucleus was more diffuse along the polar axis direction than along the normal to the 180° domain wall.